Energy & Environmental Science

www.rsc.org/ees

Volume 6 | Number 8 | August 2013 | Pages 2245–2550

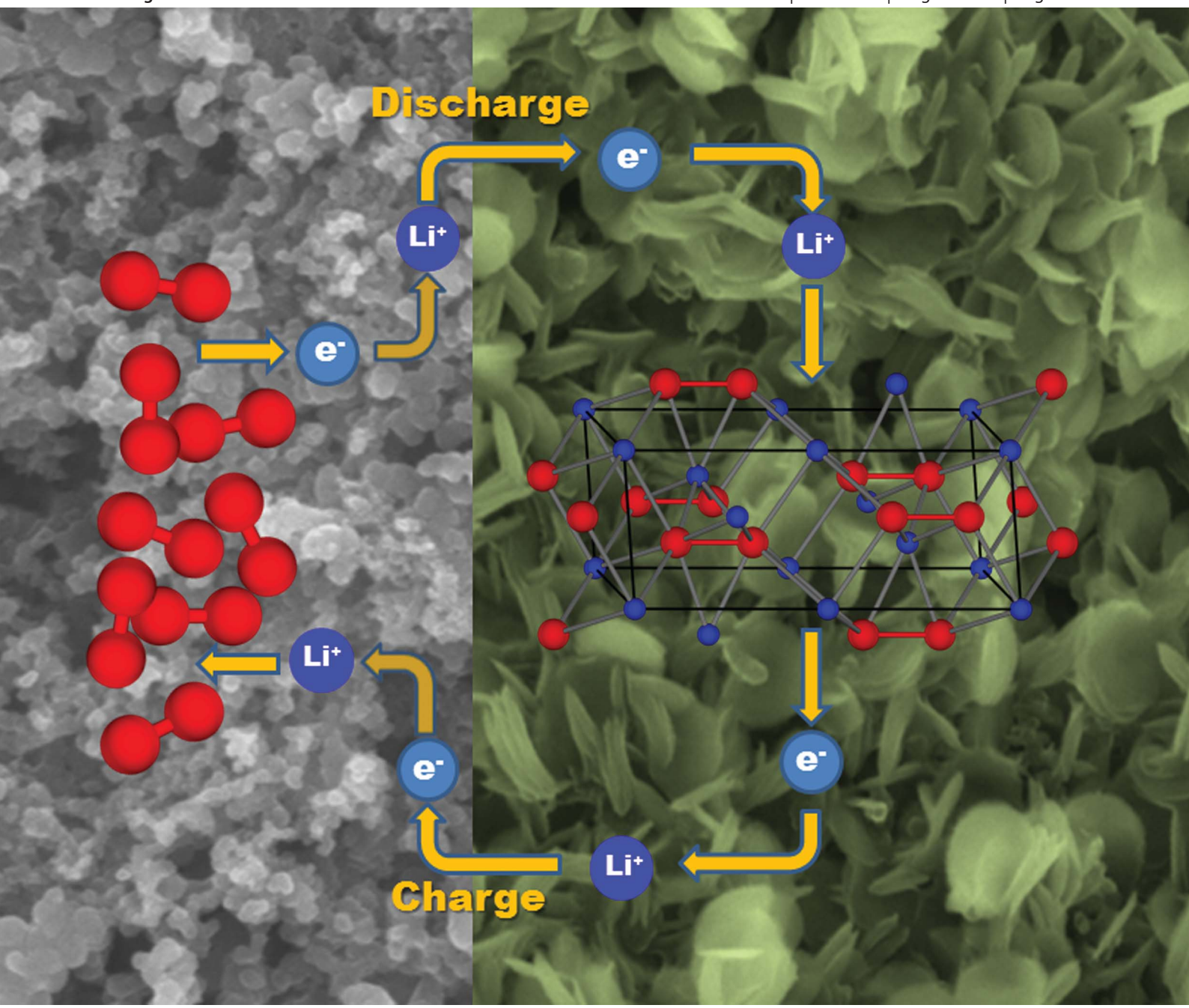

ISSN 1754-5692

RSC Publishing

PAPER

Nazar *et al.*

Na-ion mobility in layered Na_2FePO_4F and olivine $Na[Fe,Mn]PO_4$

Energy & Environmental Science

RSC Publishing

PAPER

View Article Online
View Journal | View Issue

Na-ion mobility in layered Na_2FePO_4F and olivine Na[Fe,Mn]PO_4†

Cite this: *Energy Environ. Sci.*, 2013, **6**, 2257

R. Tripathi,[a] S. M. Wood,[b] M. S. Islam*[b] and L. F. Nazar*[a]

Received 16th March 2013
Accepted 16th May 2013

DOI: 10.1039/c3ee40914g

www.rsc.org/ees

The Na-ion battery is currently the focus of much research interest due to its cost advantages and the relative abundance of sodium as compared to lithium. Olivine $NaMPO_4$ (M = Fe, $Fe_{0.5}Mn_{0.5}$, Mn) and layered Na_2FePO_4F are interesting materials that have been reported recently as attractive positive electrodes. Here, we report their Na-ion conduction behavior and intrinsic defect properties using atomistic simulation methods. In the olivines, Na ion migration is essentially restricted to the [010] direction along a curved trajectory, similar to that of $LiMPO_4$, but with a lower migration energy (0.3 eV). However, Na/M antisite defects are also predicted to have a lower formation energy: the higher probability of tunnel occupation with a relatively immobile M^{2+} cation – along with a greater volume change on redox cycling – contributes to the poor electrochemical performance of the Na-olivine. Na^+ ion conduction in Na_2FePO_4F is predicted to be two-dimensional (2D) in the interlayer plane with a similar low activation energy. The antisite formation energy is slightly higher; furthermore, antisite occupation would not be predicted to impede transport significantly owing to the 2D pathway. This factor, along with the much lower volume change on redox cycling, is undoubtedly responsible for the better electrochemical performance of the layered structure. Where volume change and structural effects do not incur impediments, Na-ion materials may present significant advantages over their Li counterparts.

Broader context

Sodium ion batteries have recently gained increased recognition as intriguing candidates for next-generation battery systems for large scale energy storage, in part owing to significant cost advantages stemming from the high natural abundance of Na resources. Although there have been limited studies on sodium analogues of the widely-reported lithium insertion materials, these have also demonstrated the possibility of significantly different structures and properties. In particular, while there have been many theoretical and experimental investigations of Li-ion migration behavior, few have analyzed the energetics of Na-ion migration. Recent studies suggest that Na-ion diffusion barriers may be as low – or even lower – than that of Li-ion in comparable alkali metal oxide materials. Our report addresses the question of why electrochemical properties of the sodium polyanion materials are often not as promising as those of their lithium counterparts, using atomistic simulation methods to probe sodium ion migration in two promising polyanion materials: olivine $NaMPO_4$ (M = Fe, $Fe_{0.5}Mn_{0.5}$, Mn) and layered Na_2FePO_4F. In both materials, activation energies for Na-ion migration are found to be quite favourable (0.3 eV), indicating that the volume expansion-induced strain on de(intercalation), which is more substantial for the larger Na^+ (*vs.* Li^+) ion, is of crucial importance in determining electrochemical properties. Indeed, very promising electrochemical properties can be anticipated for Na^+ ion materials with low volume expansion on redox, and where good electrical conduction is supported.

Introduction

The portable energy storage market has been dominated by Li-ion batteries in the past two decades due to their light-weight, high energy density and high power: which all depend critically on fast Li-ion mobility. Li-ion diffusion coefficients are often significantly high in layered transition metal oxide cathode materials such as ($LiNi_xCo_yMn_zO_2$),[1] allowing the cells to be operated at high current density during charge and discharge. Several other options for positive electrodes have been explored in last two decades, motivated by safety concerns and cost. These include "polyanion" type materials such as olivine phosphates ($LiFePO_4$),[2] tavorite fluorophosphates[3] and fluorosulfates ($LiFeXO_4F$, X = P, S).[4,5] Li-ion diffusion kinetics in these compositions depends strongly on their crystal structure. Recent studies suggest that the diffusion coefficient of Na^+ can also be very high – even higher than Li^+ – in the Na-analogues of some positive electrode materials.[6] Such systems fell by the wayside twenty years ago in favour of the higher gravimetric

[a]*Department of Chemistry, University of Waterloo, 200 University Avenue West, Waterloo, ON, N2L 3G1, Canada. E-mail: lfnazar@waterloo.ca*

[b]*Department of Chemistry, University of Bath, Bath, BA2 7AY, UK. E-mail: m.s.islam@bath.ac.uk*

† Electronic supplementary information (ESI) available. See DOI: 10.1039/c3ee40914g

capacity afforded by Li-ion cells which is critical for portable applications. However, the relative abundance and the low cost associated with Na-ion batteries now make them an attractive alternative for large-scale grid storage. Where gravimetric energy density is not a concern, Na-ion batteries are a preferable option, in fact.[7,8]

Substantial effort has been expended in previous decades to prepare electrode materials that can easily intercalate and transport Na-ions at suitable potentials. One of the challenges has been to find a good material for low-potential insertion because soft carbons are not suitable.[9,10] Important strides have been made in this area based on novel forms of hard carbons, metal alloys and a recently synthesized metal oxide $Na_2Ti_3O_7$.[10–12] Among positive electrode materials, metal oxides that include $Na_{0.44}MnO_2$,[13–15] and more recently, the highly promising P2-type $Na_x[Fe_{0.5}Mn_{0.5}]O_2$,[16] and $Na_{0.85}Li_{0.17}Ni_{0.21}Mn_{0.64}O_2$ (ref. 17) have drawn much attention. Unlike their lithium analogues, $Na_{0.5}MO_2$ layered compounds do not transform to the spinel polymorph due to the larger size of Na-ions, and hence Na_xMO_2 layered materials display improved cycling stability. Amongst the various polymorphs of Na–metal-oxides, the O3-type in which Na sits on an octahedral site, tend to be of lower practical gravimetric capacity than the P2-type that adopt a structure with Na-ions in prismatic geometry.[18,19] Electrochemical de-intercalation of Na^+ cations from these oxides occurs *via* phase transitions between multiple intermediate phases, adding to the complexity of ion-migration during charge and discharge.

Recently this topic has been examined in detail using computational studies that suggest that Na-ion migration energetics in oxides can be highly favourable.[6] These materials are being intensively investigated due to very attractive opportunities for developing low cost, high performance Na-ion positive electrode materials. Materials such as NASICON,[20] $NaVPO_4F$,[21] $NaFePO_4$ (ref. 22–24) and Na_2FePO_4F[25–27] which contain "polyanions" in their framework have also been recently investigated. Unlike the oxides, they usually display a flat voltage response upon Na-(de)intercalation due to their structural energetics that drives two-phase behavior and formation of a well-defined phase boundary between Na-rich and Na-poor phases. Their robust and stable frameworks often display better capacity retention than the oxides at the expense of slower kinetics. While there have been many theoretical and experimental studies of Li-ion migration behavior in such systems only one recent paper has analyzed the energetics of Na-ion migration.[6]

Our interest here focuses on the polyanion materials owing to their potentially more stable cycling behavior, and the insights that can be gleaned by comparing Na-ion transport in the one dimensional channels of the olivine, $NaFePO_4$, to that in the two dimensional layers of the phosphate, Na_2FePO_4F. Olivine $NaFePO_4$ can be synthesized by ion exchange from the parent lithium iron olivine.[22,23] It (de)intercalates Na-ions at 3.2 V at very slow rates of discharge. The mixed Fe–Mn system $NaFe_{0.5}Mn_{0.5}PO_4$ was also synthesized recently by direct methods,[23] and it gives a characteristically sloping electrochemical curve when cycled in a Na-ion battery. We note that conflicting reports have emerged regarding the electrochemical properties of olivine $NaFePO_4$. While the initial study by Moreau *et al.*[22] indicated that carbon coating of the parent material $LiFePO_4$ did not impact the electrochemical performance of olivine $NaFePO_4$, recent investigations by Zhu *et al.*[28] has demonstrated superior electrochemistry properties upon carbon coating ($\sim$100 mA h g^{-1} at 0.1 C rate) than that obtained previously. The performance is still inferior to that of the carbon coated lithium analogue, however.

Layered Na_2FePO_4F was first synthesized, and electrochemically investigated by Ellis *et al.*[25] The structural refinement was carried out on single crystals grown from a reaction melt. The unique ability of this structure to reversibly intercalate Li/Na ions without any significant stress stems from its robust 2D framework created by interconnected FeO_4F_2–PO_4 polyhedra that form two-dimensional slabs. Na^+ ions are nestled both near the sheets, and also between the layers in the interplanar region.[29] The interlayer cations are conserved during cycling, acting as pillars to stabilize the structure. Importantly, the material exhibits only a small volume difference (3.7%) when Na ions are de-intercalated from the 2-D layers of the structure. The initial electrochemical study demonstrated facile and reversible intercalation of Li^+ when the material was used as a cathode in a Li cell, *via* rapid exchange of Na^+ in one of the sites with Li^+. Na_2FePO_4F also intercalates Na^+-ion reversibly at an average of 3.0 V, as later demonstrated for both ionothermally,[26] and solid state[27,30] prepared materials. Capacities of about 110 mA h g^{-1} were obtained at current densities of 12.4 mA g^{-1} with as little as 1.3 wt % carbon coating using ascorbic acid as the carbon source, which also had the positive effect of reducing particle size.[30] This suggests acceptable rate capability comparable to that obtained in the Li cell, despite the larger size of the Na^+ cation.

To gain a greater understanding of the atomic-scale features influencing the electrochemical properties of layered Na_2FePO_4F and olivine $Na(Fe,Mn)PO_4$, we report here a computational study using well-established atomistic simulation methods to investigate Na-ion transport and the formation of intrinsic defects in these two contrasting materials.

Methods

The techniques are detailed elsewhere[31] (including the ESI†) and hence only a general description will be given here. Interactions between ions in the phosphate and fluorophosphate structures consist of a long-range Coulombic term and a short-range component representing electron–electron repulsion and van der Waals interactions. The short-range interactions were modeled using the two-body Buckingham potential[31] (ESI Table S1†). An additional three-body term was used for the PO_4^{3-} units to account for the angle-dependent nature of the O–P–O bonds.[32] The well-known shell model[33] was employed to account for the ionic polarizability effects. The cation–anion interactions were obtained from previous studies on phosphates[34] and fluorosulfates[35,36] with refinement of the Na–O, O–F and Na–F potentials. As argued previously, the success in employing these interatomic potential methods is assessed primarily by their ability to reproduce observed properties such as crystal structures and bond lengths. Indeed, the methods are found to work well,

even for compounds where there is undoubtedly a degree of covalency, such as aluminophosphates and olivine silicates.[37]

The lattice relaxation around defects and migrating ions was calculated by an implementation of the Mott–Littleton scheme incorporated in the GULP code.[38] This method partitions a crystal lattice into two regions, where ions in the inner region immediately surrounding the defect (greater than 700 ions) are relaxed explicitly. The relaxations of such a large number of ions are important for charge defects that introduce long-range electrostatic perturbations and are not easily treated by electronic structure methods. To calculate energy barriers of Na^+ migration, the conventional hopping model for diffusion into adjacent vacancies was used. These simulation techniques have been used successfully on a wide range of inorganic solids, including recent work on the positive electrode materials $LiFePO_4$,[39] $AFeSO_4F$[36] (A = Na, Li), $Li_2FeP_2O_7$ (ref. 40) and the negative electrode vanadate material, $LiVO_2$.[41]

Results and discussion

Structures and intrinsic defects

In the olivine $NaMPO_4$ structure (space group: *Pnma*, M = Fe, Mn), MO_6 octahedra link to each other *via* corner sharing in the *ab* plane. Sandwiched between these planes are PO_4 tetrahedra which share corners and edges with the MO_6 octahedra. This well-known framework provides open channels along the *b*-axis in which Na ions are located (Fig. 1a and b). A unique ordered composition, $Na_{0.7}FePO_4$ is also reported to form on electrochemical oxidation of $NaFePO_4$, although its precise structure has not yet been elucidated.[22] In the layered Na_2FePO_4F structure, Fe^{2+} ions are located on two crystallographic sites (Fe1 and Fe2) and coordination polyhedra around them are connected to form face-sharing bi-octahedral units. These units are connected in the *a*-direction to form Fe–F–Fe chains. The parallel chains are connected to each other by PO_4 tetrahedral units along the *c*-direction, thus forming a layer of $Fe_2O_6F_3$–PO_4 units in the *ac* plane. Na^+ ions reside in these interlayer spaces (Fig. 2a and b).

These two structures, which differ greatly in their architecture – but not too significantly in chemical composition – provide a good platform to investigate the factors underlying the observed electrochemical properties. Their calculated lattice parameters and comparison to the experimentally reported values are shown in Table 1. Lattice parameters (unit cell lengths and angles) for the three olivine (Fe, Fe/Mn, Mn) and layered compounds were simulated within a maximum difference of 1.2% from experimentally reported values. The bond lengths were also very similar. Reproduction of the lattice parameters and bond lengths provides additional validity to the interatomic potentials used for simulating defects and Na-ion migration.

Insight into the defect properties of cathode materials is crucial to the full understanding of their electrochemical behavior, especially the possibility of "blocking" anti-site defects in 1D ion conductors. The energy of formation of various types of Schottky and Frenkel defect were calculated by combining isolated vacancy and interstitial energies using the following equations (in Kröger–Vink notation):

$$\text{Na Frenkel: } Na_{Na} \rightarrow Na_i^{\cdot} + V'_{Na} \quad (1)$$

$$\text{M Frenkel: } M_M \rightarrow M_i^{\cdot\cdot} + V''_M \quad (2)$$

$$\text{Na_2O Schottky: } 2Na_{Na} + O_O \rightarrow 2V'_{Na} + V_O^{\cdot\cdot} + Na_2O \quad (3)$$

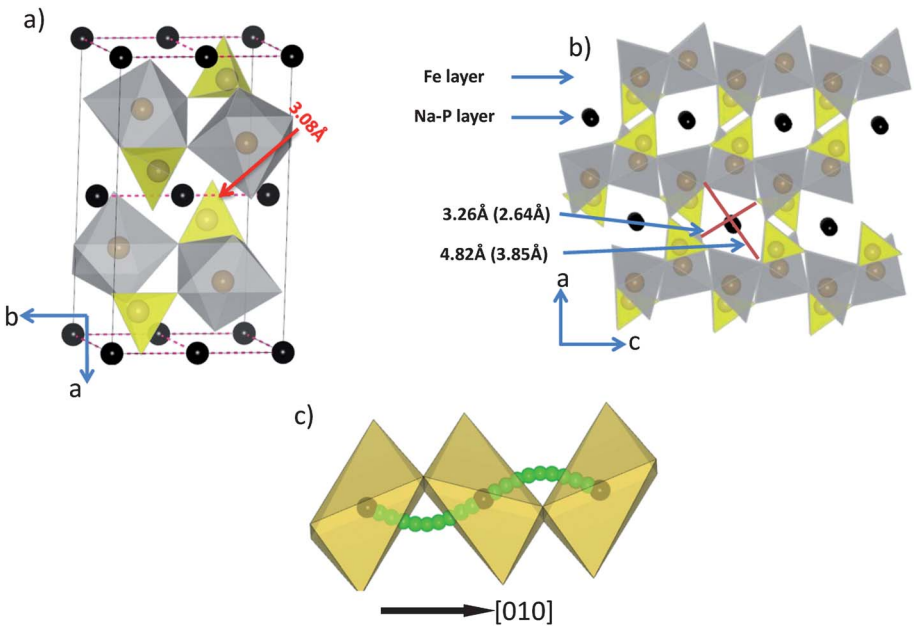

Fig. 1 (a) Unit cell of olivine $NaFePO_4$ (grey octahedra: FeO_6 and yellow tetrahedra: PO_4) and Na–Na distance along the *b*-axis; (b) tunnel dimensions for olivine $NaFePO_4$ (numbers in brackets show these lengths for isostructural $LiFePO_4$); (c) coordination octahedra around the Na-site and examples of the hop window for long range Na migration along the *b*-axis in olivine $NaMPO_4$.

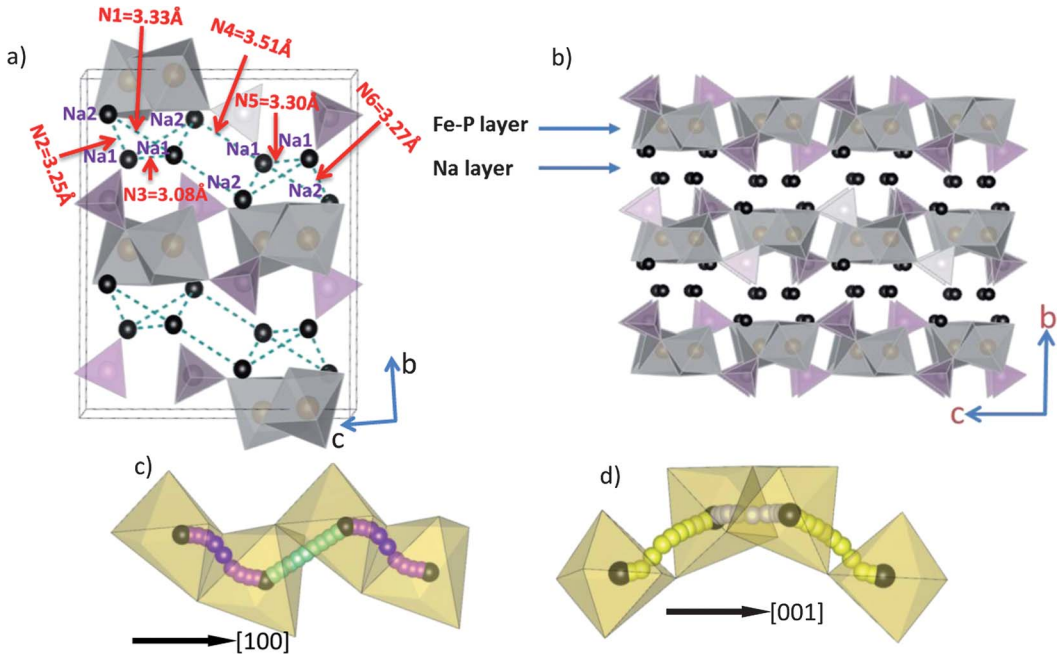

Fig. 2 (a) Unit cell of layered Na_2FePO_4F (grey octahedra: FeO_6 and pink tetrahedra: PO_4) and Na–Na distances (cutoff distance: 4 Å) (b) Fe and Na layers in layered Na_2FePO_4F. Coordination octahedra around the Na-site in Na_2FePO_4F and examples of the hop window for long range Na migration path, (c) along the *a*-axis; and (d) along the *c*-axis.

Table 1 Calculated lattice parameters for olivine $NaMPO_4$ and layered Na_2FePO_4F, and comparison to previously reported experimental values[23,25] obtained by refinement of powder X-ray diffraction patterns as indicated

Lattice parameters	*a* (Å)	*b* (Å)	*c* (Å)
$NaFePO_4$			
Experimental	10.4109	6.2283	4.9521
Calculated	10.3167	6.1635	4.9293
Δ	−0.0942	−0.0649	−0.0228
$NaMnPO_4$			
Experimental	10.5576	6.3355	4.9962
Calculated	10.6663	6.3021	4.9608
Δ	0.1087	−0.0335	−0.0353
$NaFe_{0.5}Mn_{0.5}PO_4$			
Experimental	10.4933	6.2957	4.9801
Calculated	10.4617	6.2182	4.9436
Δ	−0.0316	−0.0775	−0.0365
Na_2FePO_4F			
Experimental	5.2200	13.8540	11.7792
Calculated	5.2308	13.8469	11.7437
Δ	−0.0109	0.0084	0.0342

$$\text{NaF Schottky } (Na_2FePO_4F): Na_{Na} + F_F \rightarrow V'_{Na} + V^{\cdot}_{F} + NaF \quad (4)$$

$$\text{MO Schottky } (M = Fe,\ Mn): M_M + O_O \rightarrow V''_M + V^{\cdot\cdot}_O + MO \quad (5)$$

Anti-site defects which form by exchanging cations (Li^+/Fe^{2+}) on neighboring sites have been reported to significantly affect the electrochemical performance of the olivine $LiFePO_4$. We examined the possibility of such Na/M anti-site defect formation in both materials, which can be written as follows:

$$M_M + Na_{Na} \rightarrow Na'_M + M^{\cdot}_{Na} \quad (6)$$

Resulting defect energies for $NaMPO_4$ (M = Fe, Mn, $Fe_{0.5}Mn_{0.5}$) are listed in Table 2. The high formation energies indicate that all of the Frenkel and Schottky defects are unfavorable in olivine-type materials and would only be present in negligible concentrations in the bulk. This trend is similar to the energies of defect formation previously reported for $LiFePO_4$.[39] In contrast, antisite defects are found to have low defect energies (Table 2) which indicates that these are the most favorable type of intrinsic disorder in olivine $NaMPO_4$. Indeed, the much lower energy of formation compared to $LiMPO_4$ (0.86 *vs.* 1.13 eV (ref. 39)) is consistent with the fact that upon heat treatment, olivine $NaFePO_4$ readily transforms to the more

Table 2 Energies of formation (in eV) of intrinsic defects in olivine and layered compounds

Defects	$NaFePO_4$	$NaFe_{0.5}Mn_{0.5}PO_4$	$NaMnPO_4$	Na_2FePO_4F
Na Frenkel	2.25	2.29	2.35	3.22
Fe Frenkel	6.6	5.01	—	5.24
Mn Frenkel	—	4.91	7.28	—
Na_2O Schottky	10.05	10.06	9.71	10.78
FeO Schottky	7.31	7.48	—	5.19
FeF_2 Schottky	—	—	—	4.31
MnO Schottky	—	9.79	9.38	—
Na/Fe antisite pair (isolated)	0.86	0.86	—	1.00
Na/Mn antisite pair (isolated)	—	1.02	1.06	—

thermodynamically stable maricite phase,[42] where, compared to the olivine, the Na and Fe sites are switched in the structure:[43] *i.e.*, the alkali cation occupies the M2 site, and the transition metal occupies the M1 site. The thermodynamic preference of the maricite structure over olivine for $NaFePO_4$ has also been confirmed by computation.[6,22] Site preference is driven by a complex interplay between cation charge and size effects. In olivine $LiFePO_4$ where Li^+ ($r = 0.76$ Å) or Fe^{2+} ($r = 0.78$ Å) are effectively the same size, the higher charge on Fe^{2+} results in preference for the M2 site. However, when the size mismatch is significant, the larger cation (Na^+; $r = 1.02$ Å) is driven onto the M2 site. The different connectivity of the Fe and Na octahedra in maricite compared to olivine does not provide a free Na-ion migration pathway (as confirmed by preliminary calculations that suggest the alkali diffusion barrier is very high)[6] and results in a structure that is not amenable to Na^+ (de)insertion.

In its thermodynamically stable form, $NaMnPO_4$ adopts the maricite structure, although in another polymorph of $NaMnPO_4$, natrophilite, the M1 and M2 sites are both half occupied by Mn^{2+} (0.83 Å) and Na^+. As a result, the only method for preparing electrochemically active olivine $NaMPO_4$ relies on the topotactic conversion of olivine $LiMPO_4$ (for M = Fe) *via* a delithiation–sodiation process or a low temperature synthesis method involving a topotactic conversion of $NH_4Fe_xMn_{1-x}PO_4 \cdot H_2O$ in $NaFe_xMn_{1-x}PO_4$. The fact that direct methods cannot be used to prepare crystalline olivine $NaFePO_4$ confirms the highly metastable nature of this phase and consequently its tendency for cation disorder. The topotactic synthesis method ensures that the obtained product forms with a minimum concentration of antisite defects. However, the extraction of Na during electrochemical charge may trigger the formation of antisite defects as has been observed for $Li_{0.90}Ni_{0.45}Ti_{0.55}O_2$ obtained from $Na_{0.90}Ni_{0.45}Ti_{0.55}O_2$.[44]

In the context of ion diffusion, the antisite defects bear more significance in the case of olivine materials as their presence blocks the only available 1D channel for alkali ion migration. Therefore, anti-site defects demand that diffusion occurs *via* higher energy pathways, ultimately raising the energy barrier for Na/Li ion migration in the structure.[39] This results in the reduced power and capacity of the cathode material. For layered Na_2FePO_4F (Table 2), all the Frenkel and Schottky defects are also unfavorable. The energy of formation of antisite defects is much lower, and also comparable to that of the olivine, and suggests a small, significant percentage of Fe on Na sites and *vice versa* in the layered structure.

Na ion migration

For olivine $NaMPO_4$, we examined possible Na migration pathways already identified for Li migration in olivine $LiFePO_4$.[39] These paths are: (i) along [010], (ii) along [001], and (iii) along [101]. The path along the *b*-axis [010] provides facile channels for Na ion migration. Along the [001] path, Na^+ ions are at relatively long distances from each other and coordination polyhedra surrounding Fe and P provide a narrow window for ion migration. The path along [101] bisects the *a* and *c*-axes and passes through a narrow window formed by MO_6 and PO_4 polyhedra. Table 3a lists the calculated energies for these pathways. Activation energies along the [001] and [101] paths are relatively high (>1.5 eV), as expected from the above descriptions and are therefore unfavorable for Na^+ ion migration. This finding is similar to that reported for Li ion migration in $LiFePO_4$.[34] Interestingly, the activation energy along [010] is lower than the activation energy calculated for Li ion migration along the same direction in $LiFePO_4$ (0.55 *vs.* 0.31 eV). Our Na migration energy is very similar to that calculated by Ong *et al.*[6] using DFT methods, although they find a slightly lower Li migration energy for $LiFePO_4$, and note that the energy barrier differences for Na and Li migration are highly structure dependent.

Table 3 Na migration activation energies (in eV) of (a) olivine $NaMPO_4$. (b) layered Na_2FePO_4F

(a)

Direction	E_a ($NaFePO_4$)	E_a ($NaFe_{0.5}Mn_{0.5}PO_4$)	E_a ($NaMnPO_4$)
[010]	0.32	0.36	0.46
[001]	2.73	2.90	3.10
[101]	3.03	1.50	1.51

(b)

Direction	E_a (Na_2FePO_4F)
[100]	0.29
[001]	0.44
[010]	>2.0

Fig. 3 shows the minimum energy migration pathway for Na ions indicating a curved trajectory between Na sites along the 1D channel (rather than direct linear jumps). A very similar pathway for Li ion migration in $LiFePO_4$ was previously predicted by Islam *et al.*[39] and was subsequently confirmed by

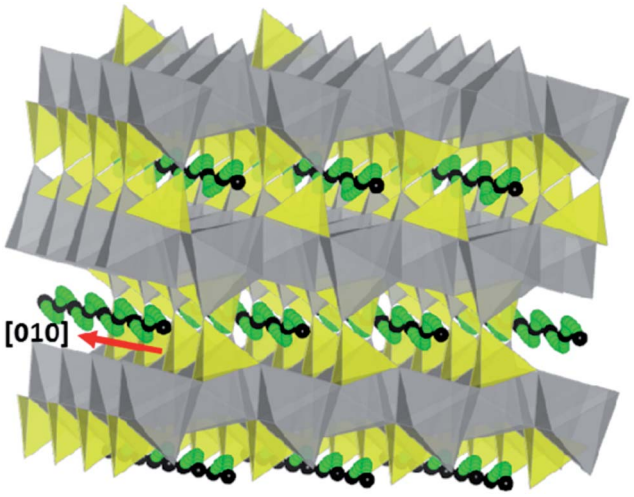

Fig. 3 Na ion migration path along the *b*-axis in olivine $NaMPO_4$. Black spheres represent Na atom sites in the olivine structures and green spheres show the most facile pathway for Na-ion hopping. MO_6 and PO_4 polyhedra are represented in grey and yellow respectively.

neutron diffraction maximum entropy methods.[45] For the mixed-metal compound $NaFe_{0.5}Mn_{0.5}PO_4$, the Na-ion migration energy barriers are slightly higher than for $NaFePO_4$ (Table 3a), but still remain slightly lower than their Li analogues (*i.e.*, $LiFe_{0.5}Mn_{0.5}PO_4$).[34]

The higher mobility of Na^+ in $NaFePO_4$ in comparison to Li^+ in isostructural $LiFePO_4$ could be attributed to much longer average lengths of Na–O bonds (2.34 Å) than Li–O bonds (1.96 Å). This suggests that the tunnels along the *b*-axis are more spacious in Na-compounds (Fig. 1b), but naturally the size of the Na^+ cation is also larger than that of Li^+. Fig. 1c shows two edge-shared NaO_6 octahedra both of which are slightly tilted towards each other thereby opening the faces below the shared edge. Such distortion adds to the space for the curved path for Na migration. In addition, it is known that polarizability effects are important as there are differences between the transport behaviour of highly polarizing cations such as Li^+ and that of less polarizing cations such as Na^+.

In contrast, the layered Na_2FePO_4F unit cell has six unique Na–Na distances (numbered N1 to N6) leading to the possible migration paths that were considered and shown in Fig. 2a. Fig. 2c and d display examples of the migration window available for Na migration along the *a* and *c*-axes. Na^+ ion polyhedra connected by hops N2 and N6 share edges with each other, whilst polyhedra connected by hop N3 and N5 share faces. Fig. 4a and b illustrate the lowest energy migration paths for Na^+ and the associated energy barriers for Na_2FePO_4F. The activation energy for inter-layer transport was also calculated, but is not shown on the diagram since its value is much higher (>2 eV).

The results (Table 3b) reveal that the lowest energy pathways in Na_2FePO_4F involve Na migration parallel to the *a*- and *c*-axes with energy barriers for long-range diffusion of about 0.3 and 0.4 eV respectively. Fig. 4 indicates that migration in the *c*-direction occurs through N4–N3–N6 hop sequences, and that migration in the *a*-direction occurs through an N3–N5 pathway. These results show that there should be high Na^+ mobility within the *a*-axis and *c*-axis channels, and 2D Na migration in the *ac* plane. This behaviour contrasts with that of $NaFePO_4$, which only allows Na^+ migration along 1D channels parallel to the *b* axis. Most importantly, ion blocking by anti-site defects is much less likely to make a significant difference to Na-ion migration in Na_2FePO_4F than it does in olivine materials exhibiting 1D diffusion. It is interesting that the calculated energy barriers in Na_2FePO_4F are almost the same as in olivine $NaMPO_4$ (~0.3 eV), but much lower than the values found for tavorite-type $NaFeSO_4F$ (>0.6 eV) using similar simulation methods.[36]

Na-de-/intercalation from Na_2FePO_4F has been observed to be much more facile than olivine $NaFePO_4$ (*vide supra*).[27,28] Given the similarity in activation energy for migration, this suggests that the volume expansion between the reduced and oxidized phases is the major contributor to determining electrochemical performance of the olivine material. All of these compounds (including tavorite $NaFeSO_4F$, which is almost electrochemically inactive) form a phase boundary between oxidized and reduced phases during charge/discharge which

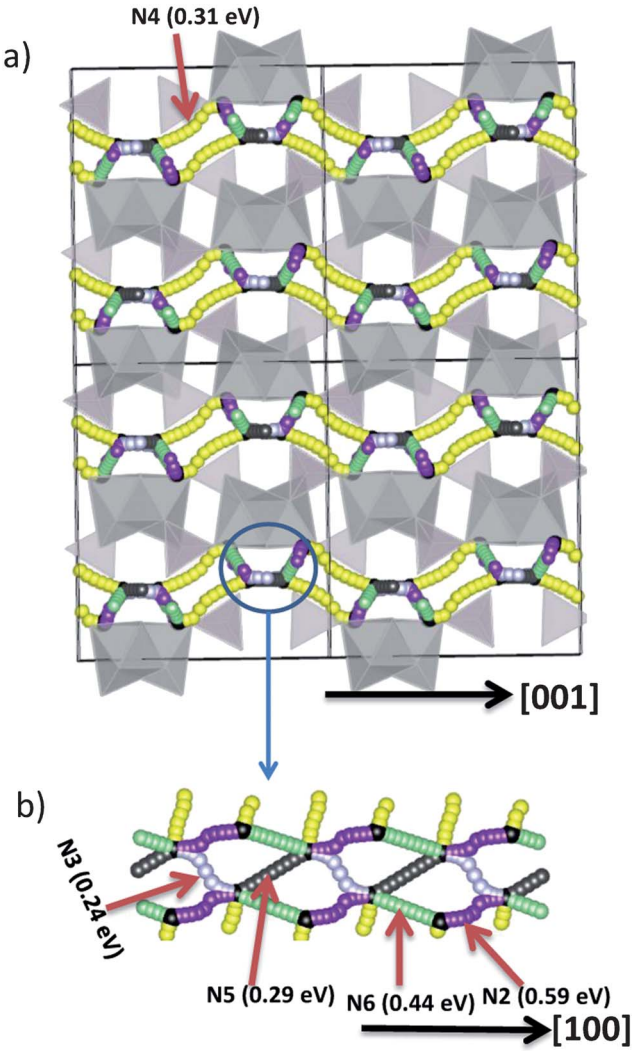

Fig. 4 Na-ion migration path along the *a* and *c*-axes in Na_2FePO_4F; octahedral FeO_4F_2 and tetrahedral PO_4 are represented by grey and yellow respectively. (a) Along the *c*-axis, the long range migration path is formed by combination of N4–N3–N6. (b) Along the *a*-direction, Na-ions migrate by a combination of N3–N5 hops.

imposes an additional activation energy barrier that corresponds to movement of the phase front in the material. Electrochemical performance is controlled by the amount of strain generated in this phase boundary, as well as by the activation energy barrier (E_a) for ion transport. Strain generated in the phase boundary is proportional to the difference in the unit cell volume (ΔV) of the oxidized and reduced phases which is ~17% for $NaFePO_4$, but only ~3.7% for Na_2FePO_4F. In the case of olivine $NaFePO_4$, it has been recently pointed out that the stress generated by formation of the phase boundary is the root cause for different electrochemical profiles during charge and discharge.[46] For the mixed transition metal phosphate $NaFe_{0.5}Mn_{0.5}PO_4$, it has been reported[23] that no phase boundary is formed upon Na de/-intercalation. However, a very large strain in the material can still be expected during the charge–discharge process, as there is about a 21% unit cell volume difference between fully oxidized and fully reduced

compositions. A large volume change between the end members also induces very significant polarization during charge and discharge as seen for olivine $NaMPO_4$.[23] In contrast, polarization is almost absent in the case of carbon coated layered Na_2FePO_4F.[27] At a moderate rate of 0.1 C, the reversible gravimetric capacity of carbon coated olivine $NaFePO_4$ and layered Na_2FePO_4F has been reported to be $\sim$110 mA h g^{-1} and $\sim$100 mA h g^{-1} respectively.[27,28] Capacities obtained after 20 cycles are almost similar for both. This is despite the lower theoretical gravimetric capacity of Na_2FePO_4F than $NaFePO_4$ based on the $Fe^{2+/3+}$ couple. While a direct comparison cannot be made in these cases due to differing carbon content/coating techniques, in general it is well accepted that a minimal volume difference on redox provides better cyclability and lower polarization. We believe this rationalizes the trend in the electrochemical performance of the polyanion families that have been studied to date: specifically $NaFeSO_4F$ (E_a = 0.60–0.91 eV, ΔV = 14.3%) > $NaFePO_4$ (E_a = 0.32 eV, ΔV = 15%) > Na_2FePO_4F (E_a = 0.30 eV, ΔV = 3.7%).

Conclusions

Our simulations show good reproduction of the observed structures of all the olivines ($NaMPO_4$) and layered (Na_2FePO_4F) materials that were investigated. The energy for antisite defect formation in olivine $NaMPO_4$ is lower than in $LiFePO_4$, suggesting a higher degree of Na on Fe sites in accordance with the known metastability of the ordered $NaMPO_4$ phases. Significantly, the activation energy barrier for Na-ion conduction in the $NaFePO_4$ olivine framework along the 1D channels is lower than for Li-ion migration in $LiFePO_4$. The Na migration barriers in the layered Na_2FePO_4F are equally favourable, indicating high Na mobility through a 2D network in the *ac* plane.

The relationship between ionic transport and electrochemical properties among these materials highlights the crucial importance of the volume expansion-induced strain on de(intercalation), which is more substantial for the larger Na^+ (*vs.* Li^+) ion. This has also been highlighted recently by others.[28] The strain contributes significantly to the overall energy for redox phase transformation, and hence materials with a high volume difference between the end member phases will invariably lead to poor rate capability and also faster capacity fade owing to electrochemical "grinding" which induces amorphization of the active material during charge and discharge. Where this is coupled with a high activation energy for Na-ion transport (*e.g.* $\geq$0.8 eV) extremely poor electrochemical properties can be predicted, an example being $NaFeSO_4F$ which exhibits almost zero intercalation capacity despite having an open tavorite-like framework that is favorable for cation migration. Intermediate volume expansion combined with good ion transport gives better, but still poor properties for 1D conductors such as $NaFePO_4$, where antisite defects present additional barriers to Na^+ diffusion. However, very promising electrochemical properties can be anticipated for Na^+ ion materials with low volume expansion on redox – and where good electrical conduction is supported – since activation energy migration barriers can be low, as in the case of Na_2FePO_4F. Although the interplay of all the above factors is clearly complex and still under investigation, these findings provide guidelines for the future design and synthesis of high rate Na-ion positive (and negative) electrodes for intercalation batteries.

Acknowledgements

L. F. N. gratefully acknowledges NSERC through funding from its Discovery, Canada Research Chair and Collaborative Research (with GM) programs. M. S. I. acknowledges funding from the EPSRC Supergen and access to Hector resources through the MCC consortium. S.M.W. acknowledges PhD funding from the DTC in Sustainable Chemical Technologies.

References

1 D. D. Mcneil, Z. Lu and J. R. Dahn, *J. Electrochem. Soc.*, 2002, **149**, A1332–A1336.
2 A. K. Padhi, K. S. Nanjundaswamy, C. Masquelier, S. Okada and J. B. Goodenough, *J. Electrochem. Soc.*, 1997, **144**, 1188–1194.
3 T. N. Ramesh, K. T. Lee, B. L. Ellis and L. F. Nazar, *Electrochem. Solid-State Lett.*, 2010, **13**, A43–A47.
4 R. Tripathi, T. N. Ramesh, B. L. Ellis and L. F. Nazar, *Angew. Chem., Int. Ed.*, 2010, **49**, 8738–8742.
5 N. Recham, J.-N. Chotard, L. Dupont, C. Delacourt, W. Walker, M. Armand and J.-M. Tarascon, *Nat. Mater.*, 2010, **9**, 68–74.
6 S. P. Ong, V. L. Chevrier, G. Hautier, A. Jain, C. Moore, S. Kim, X. Ma and G. Ceder, *Energy Environ. Sci.*, 2011, **4**, 3680–3688.
7 B. E. Ellis and L. F. Nazar, *Curr. Opin. Solid State Mater. Sci.*, 2012, **16**, 168–177.
8 V. Palomares, P. Serras, I. Villaluenga, B. K. Hueso, J. Carretero-González and T. Rojo, *Energy Environ. Sci.*, 2012, **5**, 5884–5901.
9 M. M. Doeff, Y. P. Ma, S. J. Visco and L. C. Dejonghe, *J. Electrochem. Soc.*, 1993, **140**, L169–L170.
10 D. A. Stevens and J. R. Dahn, *J. Electrochem. Soc.*, 2001, **148**, A803–A811.
11 T. T. Tran and M. N. Obrovac, *J. Electrochem. Soc.*, 2011, **158**, A1411–A1416.
12 P. Senguttuvan, G. Rousse, V. Seznec, J.-M. Tarascon and M. R. Palacín, *Chem. Mater.*, 2011, **23**, 4109–4111.
13 M. M. Doeff, M. Y. Peng, Y. P. Ma and L. C. Dejonghe, *J. Electrochem. Soc.*, 1994, **141**, L145–L147.
14 J. J. Braconnier, C. Delmas, C. Fouassier and P. Hagenmuller, *Mater. Res. Bull.*, 1980, **15**, 1797–1804.
15 J. J. Braconnier, C. Delmas and P. Hagenmuller, *Mater. Res. Bull.*, 1982, **17**, 993–1000.
16 N. Yabuuchi, M. Kajiyama, J. Iwatate, H. Nishikawa, S. Hitomi, R. Okuyama, R. Usui, Y. Yamada and S. Komaba, *Nat. Mater.*, 2012, **11**, 512–517.
17 D. Kim, S. H. Kang, M. Slater, S. Rood, J. T. Vaughey, N. Karan, M. Balasubramanian and C. S. Johnson, *Adv. Energy Mater.*, 2011, **1**, 333–336.

18 R. Berthelot, D. Carlier and C. Delmas, *Nat. Mater.*, 2011, **10**, 74–80.
19 A. Caballero, L. Hernán, J. Morales, L. Sánchez, P. J. Santos and M. A. G. Aranda, *J. Mater. Chem.*, 2002, **12**, 1142–1147.
20 J. Gaubicher, C. Wurm, G. Goward, C. Masquelier and L. F. Nazar, *Chem. Mater.*, 2000, **12**, 3240–3242.
21 J. Barker, M. Y. Saidi and J. L. Swoyer, *Electrochem. Solid-State Lett.*, 2003, **6**, A1–A4.
22 P. Moreau, D. Guyomard, J. Gaubicher and F. Boucher, *Chem. Mater.*, 2010, **22**, 4126.
23 K. T. Lee, T. N. Ramesh, F. Nan, G. Botton and L. F. Nazar, *Chem. Mater.*, 2011, **23**, 3593–3600.
24 S. M. Oh, S. T. Myungc, J. Hassound, B. Scrosati and Y. K. Sun, *Electrochem. Commun.*, 2012, **22**, 149–152.
25 B. L. Ellis, W. R. M. Makahnouk, Y. Makimura, K. Toghill and L. F. Nazar, *Nat. Mater.*, 2007, **6**, 749–753.
26 N. Recham, J.-N. Chotard, L. Dupont, K. Djellab, M. Armand and J.-M. Tarascon, *J. Electrochem. Soc.*, 2009, **156**, A993–A999.
27 Y. Kawabe, N. Yabuuchi, M. Kajiyama, N. Fukuhara, T. Inamasu, R. Okuyama, I. Nakai and S. Komaba, *Electrochemistry*, 2012, **80**, 80–84.
28 Y. Zhu, Y. Xu, Y. Liu, C. Luo and C. Wang, *Nanoscale*, 2013, **5**, 780–787.
29 B. L. Ellis, W. R. M. Makahnouk, W. N. R. Weetaluktuk, D. H. Ryan and L. F. Nazar, *Chem. Mater.*, 2010, **22**, 1059–1070.
30 Y. Kawabe, N. Yabuuchi, M. Kajiyam, N. Fukuhara, T. Inamasu, R. Okuyama, I. Nakai and S. Komaba, *Electrochem. Commun.*, 2011, **13**, 1225–1228.
31 C. R. A. Catlow, *Computer Modeling in Inorganic Crystallography*, Academic Press, San Diego, CA, 1997.
32 N. L. Allan, A. L. Rohl, D. H. Gay, C. R. A. Catlow, R. J. Davey and W. C. Mackrodt, *Faraday Discuss.*, 1993, **95**, 273–280.
33 B. G. Dick and A. W. Overhauser, *Phys. Rev.*, 1958, **112**, 90–103.
34 (*a*) C. A. J. Fisher, V. M. H. Prieto and M. S. Islam, *Chem. Mater.*, 2008, **20**, 5907–5915; (*b*) G. Gardiner and M. S. Islam, *Chem. Mater.*, 2010, **22**, 1242–1248.
35 (*a*) R. A. Jackson, M. E. G. Valerio and J. F. Lima, *J. Phys.: Condens. Matter*, 1996, **8**, 10931–10937; (*b*) M. S. Islam and S. D'Arco, *Chem. Commun.*, 1996, 2291–2292.
36 R. Tripathi, G. Gardiner, M. S. Islam and L. F. Nazar, *Chem. Mater.*, 2011, **23**, 2278–2284.
37 N. J. Henson, P. J. Hay and A. J. Redondo, *J. Phys. Chem. A*, 2000, **104**, 2423–2431.
38 J. D. Gale and A. Rohl, *Mol. Simul.*, 2003, **29**, 291–341.
39 M. S. Islam, D. J. Driscoll, C. A. J. Fisher and P. R. Slater, *Chem. Mater.*, 2005, **17**, 5085–5092.
40 J. M. Clark, S. Nishimura, A. Yamada and M. S. Islam, *Angew. Chem., Int. Ed.*, 2012, **51**, 13149–13153.
41 A. R. Armstrong, C. Lyness, P. Panchmatia, M. S. Islam and P. G. Bruce, *Nat. Mater.*, 2011, **10**, 223–229.
42 J. N. Bridson, S. E. Quinlan and P. R. Tremaine, *Chem. Mater.*, 1998, **10**, 763–768.
43 Y. Lepage and G. Donnay, *Can. Mineral.*, 1977, **15**, 518–521.
44 K. Kang, D. Carlier, J. Reed, E. M. Arroyo, G. Ceder, L. Croguennec and C. Delmas, *Chem. Mater.*, 2003, **15**, 4503–4507.
45 S. C. Nishimura, G. Kobayashi, K. Ohoyama, Y. Kanno, M. Yashima and A. Yamada, *Nat. Mater.*, 2008, **7**, 707–711.
46 M. C. Cabanas, V. V. Roddatis, D. Saurel, P. Kubiak, J. C. González, V. Palomares, P. Serras and T. Rojo, *J. Mater. Chem.*, 2012, **22**, 17421–17423.

